JSR Publications

Available Online

J. Sci. Res. **13** (2), 571-578 (2021)

JOURNAL OF SCIENTIFIC RESEARCH

www.banglajol.info/index.php/JSR

Comparatively Low Temperature Synthesis, Characterization and Some Physical Studies on Transition Metal Vanadates

T. Vaz[1*], A. V. Salker[2]

[1]Department of Chemistry, St. Xavier's College, Mapusa, Goa, India

[2]School of Chemical Science, Goa University, Goa, India

Received 8 October 2020, accepted in final revised form 31 January 2021

Abstract

Pure transition metal vanadates NiV_2O_6 and CuV_2O_6 were successfully prepared via co-precipitation technique as low as at 600 °C. The crystal structure and their phase formation were confirmed by X-ray powdered diffraction. Both the compounds were identified to have a single-phase triclinic structure. The bonding characteristics were studied by FTIR spectroscopy. The temperature dependence of electrical resistivity of these vanadates shows a typical semiconducting nature of NiV_2O_6 and CuV_2O_6, consistent with their electronic band structures. The calculated band gap energy values of NiV_2O_6 and CuV_2O_6 were found to be 2.42 and 2.0 eV respectively, employing a DRS UV-Visible spectrophotometer. Magnetic susceptibility measurements and calculated Magnetic moments confirm their paramagnetic nature. The photocatalytic efficiency was investigated by photo-degradation of methylene blue (MB) solutions employing solar light and found to be promising photocatalysts.

Keywords: Vanadates; Co-precipitation; Resistivity; Magnetism; Bandgap; Photocatalysis.

doi: http://dx.doi.org/10.3329/jsr.v13i2.49616 J. Sci. Res. **13** (2), 571-578 (2021)

1. Introduction

Vanadium oxides form a series of compounds with divalent transition metal elements of general formula $M(II)V_2O_6$ (M = Mn, Co, Ni, Cu, and Zn) commonly known as vanadates. In the present decade, vanadium based oxides have attracted much attention as anode materials in Li-ion batteries, due to their outstanding physical and chemical characteristics. The diverse crystal structures and different valence states of vanadium and also for their various V-O coordination spheres showed interesting properties. The NiV_2O_6 and CuV_2O_6 vanadates have attracted much attention owing to their valuable applications such as industrial electrodes, optoelectronics, photo-electrochemical, super-capacitors, oxidation catalysts, and more promising in rechargeable batteries [1-

* *Corresponding author*: teovaz18@gmail.com

12]. Several routes have been adopted for the synthesis of these vanadates, like conventional solid-state, hydrothermal, sol-gel route, electro-spraying, and co-precipitation methods. Though there are many newer methods, the popular conventional precipitation method to prepare NiV_2O_6 and CuV_2O_6, due to its straightforward approach has been reported in the literature [1,12-15]. The crystal structures of these compounds, depending upon the synthesis procedures have been identified [4,8,13,14]. Both NiV_2O_6 and CuV_2O_6 vanadate compounds prepared by co-precipitation method and subsequent heat treatment at 600 °C for 5 h adopt a triclinic structure at ordinary conditions [4,8,13]. Materials with semiconductor properties are known for potential photocatalysts and useful to reduce pollutants because they illustrate the simple condition to utilize natural or artificial irradiation. Though the structural properties of these vanadates have been reported earlier, there is a need for comparison of their physical properties. In this investigation, we have chosen a simple, reliable, and low-temperature co-precipitation approach to synthesize NiV_2O_6 and CuV_2O_6 materials and investigated their electrical, magnetic, and photocatalytic performances, for the envision use as anode materials in Li-ion batteries and other energy storage devices.

2. Materials and Methods

MV_2O_6 ceramics (M = Cu and Ni) were prepared by low-temperature co-precipitation route. Analytical reagent grade purity respective metal nitrates $M(NO_3)_2.nH_2O$ of Cu and Ni and ammonium vanadate were used as starting materials. All the above raw materials were used as procured. Stoichiometric amounts of raw materials were weighed and separately dissolved in a minimum quantity of pure water. The two solutions were mixed together on a magnetic stirrer. The precipitation was induced by slowly dropwise adding 1:1 ammonia solution. The pH of 8-9 was continuously maintained throughout the precipitation. After stabilization for 24 h, the precipitate was filtered, dried at 120 °C in an oven, and then sintered at 600 °C for 5 h to obtain the expected product. The product was furnace cooled, powdered, and characterized.

Structural and crystallographic analysis of prepared vanadate samples were recorded from the X-ray powder diffraction (XRD) technique using Philips X-ray diffractometer (PW 1820, Netherland) with Cu K_α radiation at room temperature. The suitable 2θ range was used. All the diffraction peaks in the observed XRD patterns can be clearly indexed by the respective I.C.D.D. files.

The Fourier Transformed Infra Red (FTIR) spectra were recorded on a Shimadzu FTIR spectrophotometer (Model 8101A, Japan) in the range of 500-1500 nm with an approximate 1 % sample supported in KBr pellet. The Diffuse Reflectance Spectroscopy was carried out to know the band gap energies of the prepared vanadates on a Shimadzu UV-2250 Spectrometer, Japan. The spectra of absorbance versus wavelength (nm) were recorded in the range of 200-800 nm at room temperature. The λ_{max} was found out by taking the first derivative plot of the reflectance spectra, the extrapolation of the mid-section of the absorbance curve was used to obtain λ_{max}. Bandgap was calculated by using the following formula, Band gap (eV) = $1240/\lambda_{max}$.

Electrical conductivity measurements were carried by a simple two-probe conductivity set-up in the temperature range of 425 to 800 K. The samples were pelletized under the pressure of 6000 Kg/cm^2, stabilized with heat treatment at 823 K for 12-14 h. The pellet was tightly held between two polished and cleaned silver electrodes and the resistivity measurements were carried out heating the assembly and recording point by point measurement. The resistivity (ρ) is then calculated from the resistance (R), surface area (A), and the thickness (l) of the pellet, using the following equation, $\rho = R \times A/l$.

The magnetic susceptibility (χ_g) in the air of these compounds was determined by the Gouy method at room temperature employing a field of the order 10,000 gauss and using $Hg[Co(SCN)_4]$ as standard material. The values of χ_g (cgs) and the magnetic moment, μ_{eff} (BM) of the paramagnetic compounds were calculated.

The photocatalytic activity of vanadate samples under investigation was tested by using a model reaction of photocatalytic degradation of methylene blue (MB) solutions, representing organic pollutants in sewage and other wastewater. The degradation was carried out with a 1×10^{-5} M dye solution containing an amount of 0.05 g of vanadate compounds. The progress of photocatalytic degradation was monitored by measuring the absorbance at the MB characteristic λ_{max} of 660 nm. The experiments were performed using sunlight. Filtered aliquots of the solutions were taken at the end of 60 min time of the irradiation and analyzed with the UV - Visible spectrophotometer. The dye degradation percentage was calculated considering initial and final concentrations of MB.

3. Results and Discussion

The compounds prepared by low-temperature co-precipitation method were characterized by recording XRD. Fig. 1 shows the XRD diffraction patterns of NiV_2O_6 and CuV_2O_6, both the compounds showed mono-phasic formation. The NiV_2O_6 and CuV_2O_6 compounds found to have triclinic structure matching with I. C. D. D. card no. 08-0329 and 30-0513 respectively. The d_{hkl} and 2θ values obtained were found to be in good agreement, the diffraction peaks were readily indexed and the absence of additional peaks, suggesting the purity of prepared samples. Comparatively the sharp diffraction peaks and high value of intensity ratio between two highest peaks indicate better crystallinity, especially for CuV_2O_6 sample. Also, the crystallite particle sizes of these compounds were calculated from the diffraction peaks data using Debye Scherrer's formula. The calculated crystallite diameters were 16.95 nm and 17.52 nm for NiV_2O_6 and CuV_2O_6 respectively confirming their nano-crystalline nature.

Fig. 2 shows IR absorption bands of NiV_2O_6 and CuV_2O_6 in the range of 500-1500 cm^{-1}. The absorption bands ranged from 500 to 950 cm^{-1}, are assigned to asymmetric or symmetric stretching vibrations of the V-O and O-V-O groups. The absorption bands at 672 and 800 cm^{-1} are assigned to the symmetric and asymmetric stretching of VO_5 units. The absorption band at 862 and 570 cm^{-1} may be assigned to V-O stretching vibration mode of V-O-V observed in both vanadates. The sharp absorption peak observed at 965

and 960 cm^{-1} are due to Ni-O-Ni and Cu-O-Cu vibrations respectively. The results are found in agreement with previous results [4,10,11,16].

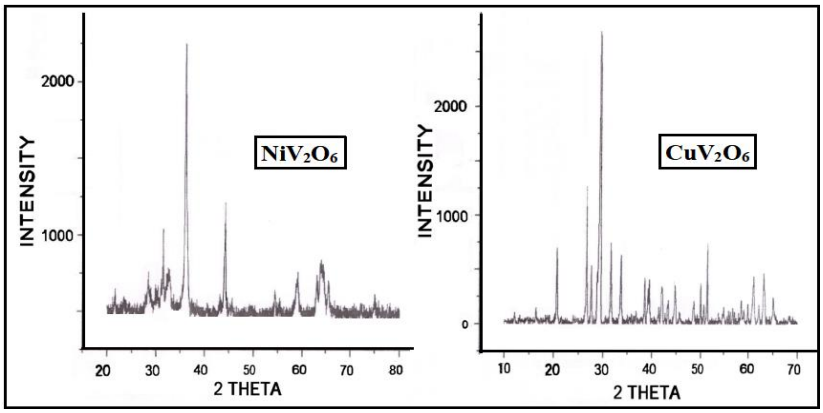

Fig. 1. XRD plots of NiV_2O_6 and CuV_2O_6.

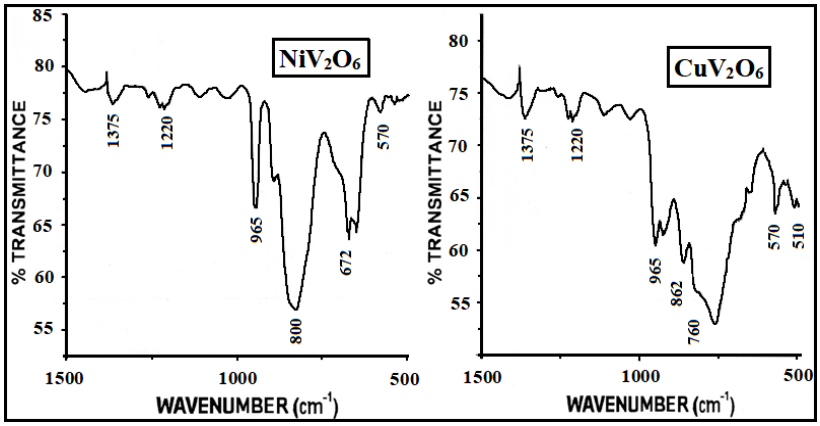

Fig. 2. IR spectra of NiV_2O_6 and CuV_2O_6 in the range of 500 - 1500 cm^{-1}.

Electrical resistivity of pelletized vanadates was measured using the two-probe method. The temperature dependence of resistivity behavior of NiV_2O_6 and CuV_2O_6 vanadates is shown in Fig. 3. For NiV_2O_6 vanadate, the resistivity measurements were recorded from 425 to 800 K. The resistivity decreases exponentially with increasing temperature, indicating typical semiconducting behavior of the materials at higher temperatures, changing to the intrinsic region in the temperature range of 550 to 600 K. At lower temperature, the resistivity pattern almost remains constant. Resistivity behavior plot of CuV_2O_6 vanadate shows nearly linear, decrease with increase in temperature from 300 to 700 K. It was noticed that around 350-400 K, region where the trend changes from

extrinsic to intrinsic behavior. In comparison to Cu ions in CuV_2O_6 vanadate, Ni ions are bit larger, resulting in a shift of extrinsic to intrinsic behavior at a higher temperature in NiV_2O_6, which is also observed in our diffused reflectance studies. The larger size of Ni ions attributes to the strong ionicity in the sample that can enhance the interaction between the anionic group and cations, in agreement with the literature [17]. To our knowledge, there are scanty literature reports available for dc resistivity measurements of these class of vanadates.

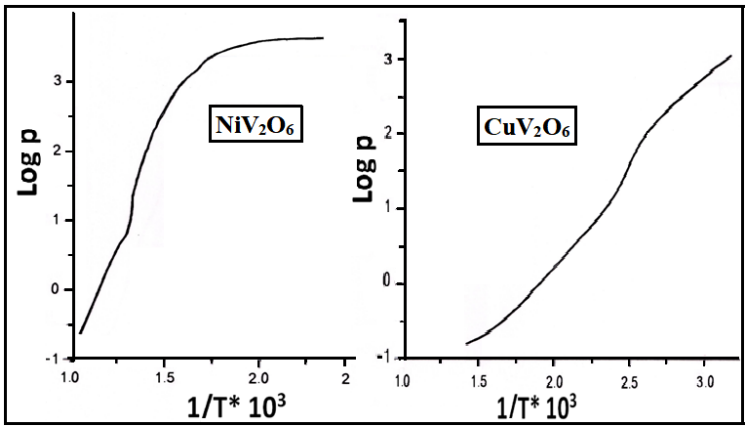

Fig. 3. Temperature dependence of resistivity for NiV_2O_6 and CuV_2O_6.

The Diffuse Reflectance Spectroscopy was carried out to understand the bandgap energies of the prepared vanadates. Fig. 4, shows the spectra of absorbance versus wavelength (nm) for NiV_2O_6, and CuV_2O_6 vanadates. The λ_{max} was found out by taking the first derivative plot of the reflectance spectra. The calculated bandgap energy values of NiV_2O_6 and CuV_2O_6 vanadates were 2.42 eV and 2.0 eV respectively, which is in agreement with the literature [4,18].

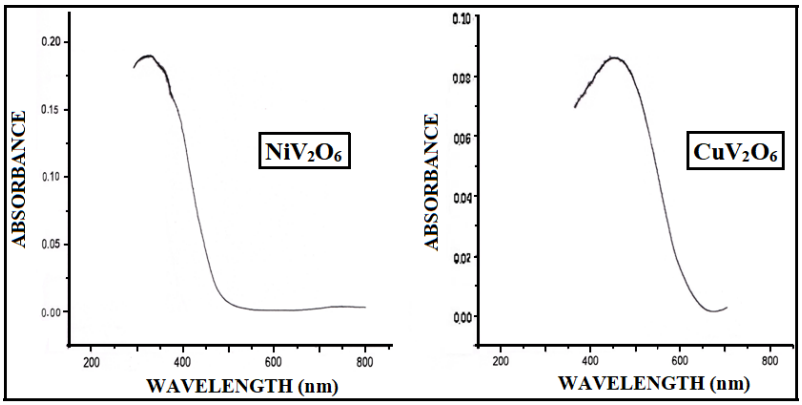

Fig. 4. Diffuse Reflectance Spectra for NiV_2O_6 and CuV_2O_6.

Table 1. Summary of the investigated work on NiV_2O_6 and CuV_2O_6 vanadates.

Compound	Crystallite diameter (nm)	Band gap energy (eV)	χ_g (cgs)	μ_{eff} (BM)	Degradation of MB (%)
NiV_2O_6	16.95	2.42	2.668×10^{-5}	4.045	83
CuV_2O_6	17.52	2.00	7.056×10^{-6}	2.1	89

The photocatalytic activity of prepared vanadates was tested by using methylene blue (MB) solution as a model reaction to study the photo-degradation of organic pollutants. Fig. 5 shows the photocatalytic degradation of MB using NiV_2O_6 and CuV_2O_6 compounds. The degradation reaction was carried out in conical flasks with stoppers containing 50 mL with 1×10^{-5} M dye solution and 0.050 g of vanadate compounds in solar light. The photocatalytic capacity of the vanadates exhibits reasonably high for degradation up to 89 %. It was clearly seen that under identical conditions, their photo-degradation efficiency within 60 min was determined to be 83 % and 89 % for NiV_2O_6 and CuV_2O_6 respectively. In order to examine the photocatalytic stability of these compounds, the experiment was repeated the next day on the same catalyst materials, the results obtained were consistent.

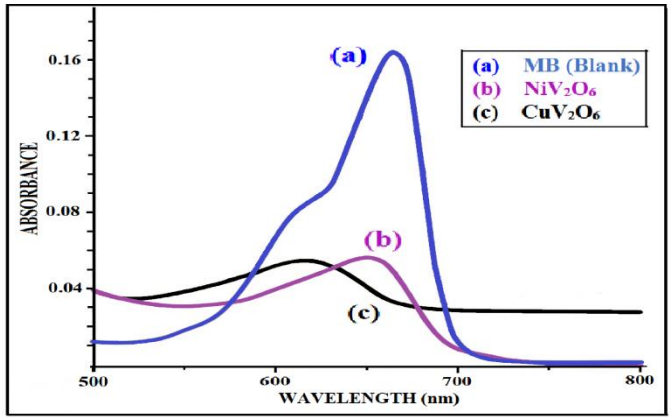

Fig. 5. Photo-catalytic degradation of MB on NiV_2O_6 and CuV_2O_6.

The higher photocatalytic activity of CuV_2O_6 could be attributed to its stronger Visible light absorption. As observed in Fig. 5, the MB degradation percentage on vanadates increased rapidly, after the reaction mixture kept in direct sunlight between 11.00 am to 12.00 noon and within 60 min, it was noted appreciable degradation, as indicated by fading of dye color, almost too colorless. These results indicate that prepared transition metal vanadates have potential and efficiency for photocatalytic applications. The photocatalytic capacity of these vanadates may be due to larger surface area, owing to finer crystallite particle size, as observed from XRD patterns prepared by low-temperature co-precipitation precursor technique. In addition, the smaller band gap energy of CuV_2O_6 vanadate may be the reason for superior photocatalytic nature. These vanadates are also reported as visible light active metal oxides [17], thus their chemical activity is significantly favoring their suitability for photocatalytic degradation of organic pollutants.

4. Conclusion

Crystalline NiV_2O_6 and CuV_2O_6 vanadates have been successfully prepared through co-precipitation precursor method at 600 °C and indexed to the triclinic structure. The temperature-dependent dc resistivity shows typical semi-conductor behavior, which is consistent with the calculated electronic band gap energies. The band gap energy of NiV_2O_6 is higher than CuV_2O_6 material, attributed to the size difference of Ni and Cu atoms. From the values of magnetic susceptibility and calculated magnetic moments, it is inferred that both compounds are paramagnetic in nature. The photocatalytic behavior of these vanadates shows that they have efficient degradation capacity for methylene blue resembling organic pollutants, with the superior activity of CuV_2O_6.

Acknowledgment

The authors are grateful to D. Adonkar, for the help in these investigations.

References

1. E. Andrukaitis, J. P. Cooper, and J. H. Smit, J. Power. Sources **54**, 465 (1995). https://doi.org/10.1016/0378-7753(94)02126-N
2. M. Eguchi, T. Iwamoto, T. Miura, and T. Kishi, Solid State Ion. **89**, 109 (1996). https://doi.org/10.1016/0167-2738(96)00259-7
3. M. S. Islam, H. Kabir, Y. Inagaki and A. R. Sarker, J. Alloys Compds. **829**, 154499 (2020). https://doi.org/10.1016/j.jallcom.2020.154499
4. M. A. Rahman, M. R. Akter, M. R. Khatun, R. Sultana, and M. A. R. Sarker, Phys. Solid State **62**, 1024 (2020). https://doi.org/10.1134/S1063783420060049
5. S. Hikazudani, K. Kikutani, K. Nagaoka, T. Inoue, and Y. Takita, Appl. Catal. A: Gen. **345**, 65 (2008). https://doi.org/10.1016/j.apcata.2008.04.022
6. M. W. Kim, B. Joshi, H. Yoon, T. Ohm, K. Kim, S. S. Al-Deyab, and S. S. Yoon, J. Alloys Compds. (2017). https://doi.org/10.1016/j.jallcom.2017.02.302
7. C. Jun-qi, W. Xian-you, T. Anping, W. Xin, W. Ying, and W. Wen, J. Alloys Compds. **479**, 875 (2009).
8. S. Zhang and R. Hu, Mater. Lett. **176**, 131 (2016). https://doi.org/10.1016/j.matlet.2016.04.108
9. G. Han, S. Yang, Y. Huang, J. Yang, W. Chai, R. Zhang, and D. Chen, Trans. Nonferrous Met. Soc. **27**, 1105 (2017). https://doi.org/10.1016/S1003-6326(17)60129-8
10. B. J. Rani, G. Ravi, R. Yuvakkumar, M. P. Kumar, S. Ravichandran, D. Velauthapillai, M. Thambidurai, and C. Dang, Mater. Lett. **274**, ID 127996 (2020). https://doi.org/10.1016/j.matlet.2020.127996
11. M. Isacfranklin, C. Deepika, G. Ravi, R. Yuvakkumar, D. Velauthapillai, and B. Saravanakumar, Ceram. Int. (2020). https://doi.org/10.1016/j.ceramint.2020.07.320
12. M. K. Hossain, P. Sotelo, H. P. Sarker, M. T. Galante, A. Kormanyos, C. Longo, R. T. Macaluso, M. N. Huda, C. Janáky, and K. Rajeswar, ACS Appl. Energy Mater. (2019). https://doi.org/10.1021/acsaem.9b00179
13. Wei, K. W. Nam, G. Chen, C. W. Ryu, and K. B. Kim, Solid State Ion. **176**, 2243 (2005). https://doi.org/10.1016/j.ssi.2005.06.018
14. E. Baudrin, M. Touboul, and G. Novogrocki, J. Sol. St. Chem. **152**, 511 (2000).
15. S. Akhtar, M. A. Alam, and H. Ahmad, J. Sci. Res. **9**, 413 (2017). https://doi.org/10.3329/jsr.v9i4.32726

16. K. Hua, X. Xu, D. Fang, R. Bao, Z. Fu, J. Hu, et al, J. Magn. Magn. Mater. **473**, 435 (2019). https://doi.org/10.1016/j.jmmm.2018.10.105
17. H. X. Dang, A. J. E. Rettie, and C. B. Mullins, J. Phys. Chem. C **119**, 14524 (2014). https://doi.org/10.1021/jp508349g
18. Y. Huang, X. Meng, P. Gong, L. Yang, Z Lin, X. Chen, and J. Qin, J. Mater. Chem. C **2,** 4057 (2014). https://doi.org/10.1039/C4TC00264D